Mössbauer spectroscopy and neutron diffraction studies of the compound $YSrCuFeO_{5+y}$

1998 J. Phys.: Condens. Matter 10 10317

(http://iopscience.iop.org/0953-8984/10/45/018)

J. Phys.: Condens. Matter **10** (1998) 10317–10332. Printed in the UK PII: S0953-8984(98)94593-3

Mössbauer spectroscopy and neutron diffraction studies of the compound $YSrCuFeO_{5+y}$

M Pissas†, G Kallias†, A Simopoulos†, D Niarchos†, E Devlin† and R Sonntag‡§

† Institute of Materials Science, National Centre for Scientific Research Demokritos 153, 10 Aghia Paraskevi, Attiki, Greece

‡ Berlin Neutron Scattering Centre, Hahn-Meitner-Institut, Glienicker Strasse 100, D-14109 Berlin, Germany

Received 26 May 1998

Abstract. We have studied the crystal structure and the magnetic properties of the oxygen-deficient perovskite $YSrCuFeO_{5+y}$ using x-ray and neutron powder diffraction, and ^{57}Fe Mössbauer spectroscopy. The neutron diffraction data have shown antiferromagnetic long-range order described with two propagation vectors $\boldsymbol{k}_1 = (1/2, 1/2, 1/2)$ and $\boldsymbol{k}_2 = (1/2, 1/2, 1)$. Mössbauer spectroscopy for $T > T_N$ ($T_N = 397 \pm 5$ K) revealed the existence of two Fe local environments. The first one (85% of the spectral area) was attributed to fivefold-oxygen-coordinated Fe^{3+} ($S = 5/2$) and the second to octahedrally coordinated Fe^{3+} ($S = 5/2$). For $T < T_N$ the spectra are magnetically split and can be analysed with a distribution of H_{eff}. The relation of the second Mössbauer site to the second propagation vector $\boldsymbol{k}_2$ and to the amount of additional oxygen in the $(\frac{1}{2}, \frac{1}{2}, \frac{1}{2})$ position is examined.

1. Introduction

The study of antiferromagnetic compounds which are structurally related to the high-T_c superconductors is of great importance in the effort to understand their crystal chemistry, phase stability and magnetic properties. The family R(Ba, Sr)(A, B)O_{5+y} (where R = rare earth, Y and La, and A, B are transition metals) display a wide variety of properties related to crystal chemistry and antiferromagnetic interactions. Among the great number of these compounds, $YBaCuFeO_{5+y}$ is an interesting material because of the simplicity of its structure and the fact that it is nearly stoichiometric as regards the oxygen, i.e. it readily retains the 'O_5' composition for samples quenched in air. The structure of $YBaCuFeO_5$ (figure 1) can be derived from that of $YBa_2Cu_3O_{6+y}$ by eliminating the CuO chain levels [1]. Mössbauer spectroscopy revealed a single Fe site which was attributed to Fe^{3+} ($S = 5/2$). The Fe moments make a 68° angle with the c-axis and are antiferromagnetically ordered with the Néel temperature $T_N = 446$ K. In addition, $YBaCuFeO_{5+y}$ shows a novel magnetic phase transition [2, 3] at 190 K where two sets of satellite peaks surround the (1/2, 1/2, 1/2) magnetic peak, collapsing into a single set [3] of satellites below 155 K.

Searching for the interplay between the crystal chemistry and the magnetic properties of the 'model' mixed perovskites crystals R(Ba, Cu)(Cu, $Fe)_2O_{5+y}$, we have studied the compound $YSrCuFeO_{5+y}$. Its magnetic properties differ significantly from those of the

§ Also at: Institute for Crystallography, University of Tübingen, D-72070 Tübingen, Germany.

0953-8984/98/4510317+16$19.50

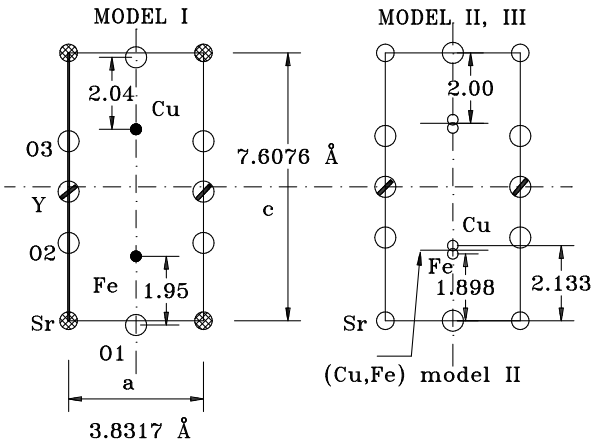

Figure 1. The crystal structure of the $YSrCuFeO_{5+y}$ compound.

isostructural compound $YBaCuFeO_{5+y}$. That is, the commensurate-to-incommensurate magnetic transition is absent in $YSrCuFeO_{5+y}$. Across the whole temperature range studied, the $YSrCuFeO_{5+y}$ compound exhibits a magnetic structure which can be described with two propagation vectors. It may be the case that the incommensurate magnetic structure present in $YBaCuFeO_{5+y}$ changes into a non-collinear one. A brief report on its magnetic structure has been given in reference [4].

In this paper we report neutron diffraction and Mössbauer spectroscopy data on $YSrCuFeO_{5+y}$ for the temperature range 2–450 K. These results are compared with recent data for the isostructural $ReBaCuFeO_{5+y}$ (Re = Y, Pr) compounds. We also try to explain the observed behaviour, taking into account the extra oxygen located in the Y layers.

2. Experimental methods

A sample with nominal composition $YSrCuFeO_5$ was prepared by thoroughly mixing high-purity stoichiometric amounts of $SrCO_3$, CuO, Fe_2O_3 and Y_2O_3. The mixed powders were pelletized and annealed in air at 980 °C for several days with intermediate grindings and reformation into a pellet each time. Finally, the sample was quenched to room temperature (RT). It is worth noting the phase evolution during the reaction process at 980 °C. $YSrCuFeO_5$ and $Sr_3Fe_2O_{7-y}$ are formed first and with the passage of time the amount of $YSrCuFeO_5$ increases with respect to that of $Sr_3Fe_2O_{7-y}$. During the first stages of the reaction a small amount of $Y_2Cu_2O_5$ is formed and remains thereafter. X-ray powder diffraction patterns were taken in the Bragg–Brentano geometry (from 20° to 120° with a step of 0.03°) with Cu Kα radiation using a graphite crystal monochromator (Siemens D500). Mössbauer spectra were recorded using a conventional constant-acceleration spectrometer with a ^{57}Co(Rh) source moving at RT while the absorber was kept fixed at the desired temperature. DC magnetization measurements were performed using a SQUID magnetometer (Quantum Design).

The neutron powder diffraction (NPD) experiments were performed in the flat-cone E2 and E6 focusing single-crystal diffractometer of the research reactor BERII in Berlin. The (311) reflection of the Ge monochromator with wavelength $\lambda \approx 1.2$ Å and the (002) reflection of the pyrolytic graphite monochromator with wavelength $\lambda \approx 2.4$ Å were used.

3. Crystal structure refinement

In view of earlier structural work on other isostructural compounds [3, 5, 6], three structural models were considered:

(a) fully ordered structure in which the Fe^{3+} and Cu^{2+} ions occupy distinct crystallographic sites (space group $P4mm$—model I);

(b) completely disordered structure with the Fe^{3+} and Cu^{2+} ions randomly distributed in the (Cu, Fe)O_2 layers (space group $P4/mmm$—model II); and

(c) partially disordered structure which has the same crystal structure as model II, except that $z_{Fe} \neq z_{Cu}$ (space group $P4/mmm$—model III).

In $YBaCuFeO_{5+y}$, single-crystal structural analysis [7], Mössbauer spectroscopy [8, 9], magnetic neutron diffraction [10, 3] and Raman and IR spectroscopic studies [11] have shown that the correct structural description must be based on the $P4mm$ space group.

Table 1. Fractional atomic coordinates and isotropic temperature factors, for the compound $YSrCuFeO_{5+y}$, obtained using neutron diffraction data at $T = 300$ K. Rietveld refinements were done in the tetragonal space group $P4mm$ (model I), $P4/mmm$ (model II) and $P4/mmm$, $z_{Fe} \neq z_{Cu}$ (model III). The atom positions are: Y: $(0, 0, z)$; Sr: $(0, 0, 0)$; Fe: $(1/2, 1/2, z)$; Cu: $(1/2, 1/2, z)$; O1: $(1/2, 1/2, z)$; O2: $(1/2, 0, z)$; O3: $(1/2, 0, z)$; O4: $(1/2, 1/2, 1/2)$.

	NPD data $a = 3.8317(1)$ Å $c = 7.6076(4)$ Å		
Atom	Model I	Model II	Model III
z(Sr)	0	0	0
B(Sr)	1.4(2)	2.2(1)	2.15(1)
z(Y)	0.486(4)	1/2	1/2
B(Y)	0.3(1)	0.38(8)	0.27(8)
z(Fe)	0.240(2)	0.2631(4)	0.249(1)
B(Fe)	0.33(6)	0.33(5)	0.04(7)
z(Cu)	0.714(2)	0.2631(4)	0.280(1)
B(Cu)	0.33(6)	0.33(5)	0.04(7)
z(O1)	−0.016(4)	0	0
B(O1)	1.17(7)	1.10(5)	1.08(5)
z(O2)	0.290(4)	0.3105(3)	0.3103(4)
B(O2)	1.17(7)	1.10(5)	1.08(5)
z(O3)	0.670(4)	—	—
B(O3)	1.17(7)	2.1(1)	2.1(1)
O4	0.486(4)	1/2	1/2
B(O4)	1.17(7)	1.10(5)	1.08(5)
n(O4)%	7(1)	8(1)	6(1)
R_p	5.03	5.04	4.99
R_{wp}	6.47	6.49	6.38
R_B	5.42	5.30	5.53

The refinement of the XRD patterns was carried out by the BBWS-9006 Rietveld program [12], while for the NPD patterns we used the profile-fitting program FULLPROF [13]. The profile shape function was assumed to be Pearson VII for the x-ray data, while for neutrons we used a pseudo-Voigt function with the mixing parameter $\eta = 0.3$. The background was refined together with the structure. We used the XRD data for phase identification and cell constant estimation. The refined parameters for all three structural

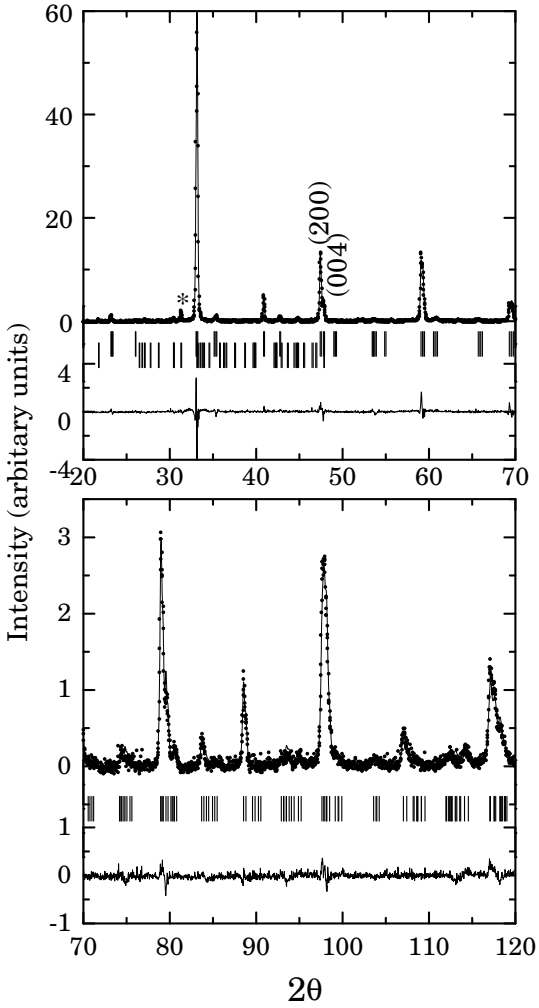

Figure 2. The Rietveld refinement pattern for powder x-ray diffraction data for $YSrCuFeO_{5+y}$. The observed intensities are shown by dots and the calculated ones by solid lines. The positions of the Bragg reflections are shown by the small vertical lines below the patterns. The upper vertical lines are for the reflections of $YSrCuFeO_{5+y}$, while the lower ones are for the reflections of $Y_2Cu_2O_5$. The asterisk at 31.3° denotes the more intense peak of the $Y_2Cu_2O_5$ phase. The line at the bottom indicates the intensity difference between the experimental and the refined patterns.

models obtained using the NPD data are listed in table 1. Figure 2 and figure 3 show the refined XRD and PND patterns at $T = 300$ K, respectively. The sample consists of a single phase except for a reflection of small intensity (less than 5% of the more intense peak) at 31.3° in the XRD pattern, which probably comes from $Y_2Cu_2O_5$. The lattice parameters a and c are reduced by 0.35 and 0.6 Å respectively with respect to those of $YBaCuFeO_{5+y}$. This decrease can be attributed to the fact that the ionic radius of Sr in dodecahedral coordination is smaller than that of Ba by 0.17 Å [14].

Satisfactory refinements of the nuclear structure were obtained for all models although the reliability factors (mainly R_B) are slightly better for model III. However, no safe

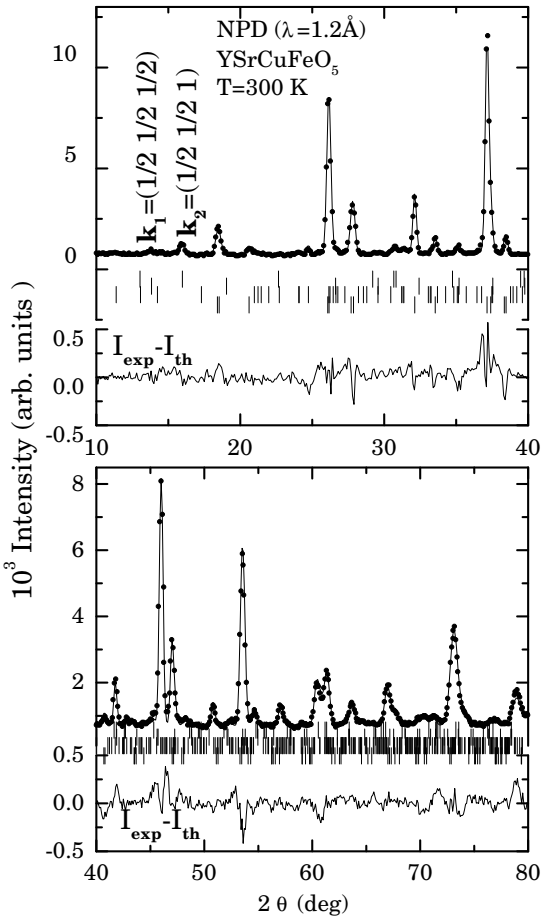

Figure 3. Rietveld refinement patterns at RT for an YSrCuFeO$_{5+y}$ sample obtained using neutron powder diffraction data ($\lambda = 1.221$ Å). The observed intensities are shown by dots and the calculated ones by solid lines. The positions of the Bragg reflections are shown by the small vertical lines below the patterns. The upper two denote the reflections that correspond to the propagation vectors $\boldsymbol{k}_2$ and $\boldsymbol{k}_1$ respectively, the third to the nuclear part of YSrCuFeO$_{5+y}$ and the fourth to $Y_2Cu_2O_5$. The line at the bottom indicates the intensity difference between the experimental and the refined patterns.

conclusion can be drawn from this. The improvement in the refinement on going from models I and II to III is not statistically significant on the basis of the nuclear profile refinements. For model I the fit was a little better when Cu^{2+} was at the centre of the severely elongated pyramid (Cu–$O_{ax} = 2.04(4)$ Å, Cu–$O_{eq} = 1.945(6)$ Å). In the FeO_5 pyramid the Fe–O_{ax} bond distance (1.95(4) Å) is shorter than the Fe–O_{eq} distances (1.953(6) Å), with the iron ion ≈0.36 Å above the basal plane of the pyramid. On the other hand, model II leads to a (Cu/Fe)O_5 pyramid with the apical distance (2.00(1) Å) appreciably larger than the equatorial distance (1.949(8) Å). Finally, in model III there are two types of pyramid as in model I. For the iron pyramid, Fe–$O_{ax} = 1.89(1)$ Å and Fe–$O_{eq} = 1.971(2)$ Å, while for copper, Cu–$O_{ax} = 2.133(1)$ Å and Cu–$O_{eq} = 1.929(1)$ Å.

In other Fe-substituted cuprate perovskites, with Fe and Cu occupying a site with

pyramidal coordination, the apical (Cu/Fe)–O_{ax} bond distance is larger than the equatorial (Cu/Fe)–O_{eq} distance. In (Y, Ce)$_2$Sr$_2$Cu$_2$FeO$_{10-y}$ the corresponding distances are 2.02(2) and 1.919 Å [15], in YSr$_2$Cu$_{3-x}$Fe$_x$O$_y$ they are 2.10(1) and 1.922 Å [16] and in Y$_2$SrCuFeO$_{6.5}$ they are 2.002(2) and 1.968(6) Å [17]. However, in compounds where Cu and Fe occupy different crystallographic sites with pyramidal coordination, the Fe–O_{ax} bond distance is shorter than the Fe–O_{eq} distance. For example, in YBaCuFeO$_{5+y}$ it is Fe–O_{ax} = 1.82(9) Å and Fe–O_{eq} = 2.03(3) Å [10]. Also, in (Y, Ce)$_2$Sr$_2$CuFeO$_8$ [18] it is Fe–O_{ax} = 1.855(1) Å and Fe–O_{eq} = 1.923(1) Å [18].

All models revealed ≈6% occupancy at the (1/2, 1/2, 1/2) oxygen position. This oxygen is also seen in the Mössbauer spectra, since it changes the iron coordination from square pyramidal to octahedral, thereby increasing the electric field gradient.

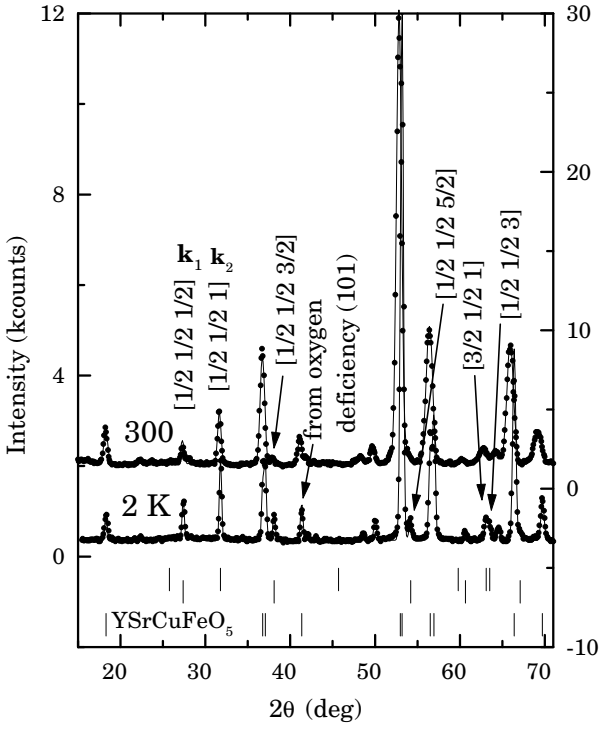

Figure 4. Rietveld refinement patterns at 300 K (instrument E2 (low resolution)) and 2 K (instrument E6) for an YSrCuFeO$_{5+y}$ sample obtained using neutron powder diffraction data (λ = 2.41 Å). The positions of the Bragg reflections are shown by the small vertical lines below the pattern. The upper two denote the reflections that correspond to the propagation vectors $\boldsymbol{k}_2$ and $\boldsymbol{k}_1$ respectively and the lower ones to the nuclear part of YSrCuFeO$_{5+y}$. The observed intensities are shown with dots and the calculated ones with the solid lines.

4. Magnetic structure

Figure 4 shows the neutron diffraction patterns at 300 K and 2 K. Apart from the expected crystal structure peaks there are additional peaks that are absent from the corresponding XRD patterns. Moreover, since their intensities decrease with increasing temperature these peaks can be attributed to magnetic long-range order. The magnetic peaks can be indexed

with superlattice indices $(h_1/2, k_1/2, l_1/2)$ and $(h_2/2, k_2/2, l_2)$, where $h_1, k_1, h_2, k_2, l_1, l_2$ are odd integers. The $(h_1/2, k_1/2, l_1/2)$ reflections come from a spin arrangement with propagation vector $\boldsymbol{k}_1 = [\frac{1}{2}, \frac{1}{2}, \frac{1}{2}]$. The half-integer indices imply that $\boldsymbol{S}(\boldsymbol{R} + \boldsymbol{c}) = -\boldsymbol{S}(\boldsymbol{R})$ and $\boldsymbol{S}(\boldsymbol{R} + \boldsymbol{a}) = -\boldsymbol{S}(\boldsymbol{R})$ (or $\boldsymbol{S}(\boldsymbol{R}) = \exp(\mathrm{i}\boldsymbol{k}_1 \cdot \boldsymbol{R})\boldsymbol{S}(0)$), where $\boldsymbol{R}$ is a lattice vector and $\boldsymbol{S}(\boldsymbol{R})$, $\boldsymbol{S}(\boldsymbol{0})$ are the magnetic moments at the lattice sites $\boldsymbol{R}$ and $\boldsymbol{0}$, respectively. The $(h_2/2, k_2/2, l_2)$ reflections come from a spin arrangement with propagation vector $\boldsymbol{k}_2 = [\frac{1}{2}, \frac{1}{2}, 1]$, which implies that $\boldsymbol{S}(\boldsymbol{R} + \boldsymbol{c}) = \boldsymbol{S}(\boldsymbol{R})$ and $\boldsymbol{S}(\boldsymbol{R} + \boldsymbol{a}) = -\boldsymbol{S}(\boldsymbol{R})$. According to the above remarks there are three possible candidate collinear magnetic models for $\boldsymbol{k}_1$ and only one for $\boldsymbol{k}_2$. Since the half-integer and integer Bragg reflections correspond to separate Fourier components they can be treated separately. We may then solve for the components of the spin structure for the two types of reflection separately. The overall picture can be interpreted with two models:

(a) an *incoherent mixture of domains* with different propagation vectors and with the same ordered moment, but occupying different volumes; and

(b) a *canted model* which is the vector sum of two collinear magnetic structures with different ordered magnetic moments but occupying the same volume [19].

According to Rossat-Mignod [20], the reason for the existence of a canted magnetic structure is the existence of terms higher than second order in the magnetic free-energy expression.

The magnetic structure factor for $\boldsymbol{k}_1$ on the basis of a magnetic unit cell with $a_M = b_M = \sqrt{2}a_N, c_M = 2c_N$ is

$$F(hkl) = (1 - \mathrm{e}^{\pi\mathrm{i}(h+k)})(1 - \mathrm{e}^{\pi\mathrm{i}l})(p_A\mathrm{e}^{2\pi\mathrm{i}lz} + \mathrm{e}^{\pi\mathrm{i}l}p_B\mathrm{e}^{-2\pi\mathrm{i}lz}) \tag{1}$$

where $p_j = (\text{occupancy}) \times (0.269 \times 10^{-12}\ \mathrm{cm}/\mu_B) S_j f_j \exp(-W_j)$. S_j is the average ordered magnetic moment (in Bohr magnetons, μ_B) for the jth atom in the j-layer ($j = \mathrm{A}, \mathrm{B}$), f_j is the magnetic form factor [21] for the magnetic ion at the jth layer and W_j is the Debye–Waller factor for the jth atom. For p_A and p_B it can be either $p_A = p_B$ or $p_A = -p_B$. However, there is practically no difference between the calculated patterns of the two models (because according to equation (1) for $z \approx 1/4$, $F^2 \propto 4p_A^2 \sin^2(\pi/4)$ or $F^2 \propto 4p_A^2 \cos^2(\pi/4)$ for $p_A = p_B$ and $p_A = -p_B$ respectively), so we cannot distinguish between them. A refinement performed with the magnetic moment lying in the a–b plane gave poor agreement. A better result was obtained by considering that the magnetic moment is directed along the c-axis. Considerable improvement was achieved with the magnetic moment at an angle to the c-axis. These results were obtained upon comparing the intensity ratio of the peaks (1/2 1/2 3/2) and (1/2 1/2 1/2), which depends only on the orientation factor $\langle 1 - (\hat{\boldsymbol{q}} \cdot \hat{\boldsymbol{s}})^2 \rangle_{\{hkl\}}$ and not on the magnitude of the magnetic moment.

Similarly, the structure factor for $\boldsymbol{k}_2$ on the basis of the magnetic unit cell with $a_M = b_M = \sqrt{2}a_N, c_M = c_N$ is

$$F(hkl) = (1 - \mathrm{e}^{\pi\mathrm{i}(h+k)})(p_A\mathrm{e}^{2\pi\mathrm{i}lz_A} + p_B\mathrm{e}^{-2\pi\mathrm{i}lz_B}). \tag{2}$$

The absence of the $l = 0$ magnetic Bragg peak implies that the sum of the spins of two adjacent layers is zero, which in turn means that the magnetic moments of these layers are of equal magnitude but in opposite directions ($p_A = -p_B$). This situation cannot be realized unless layers A and B are equivalent. Taking $z_B = 1 - z_A$, the structure can be written as

$$F(hkl) = (1 - \mathrm{e}^{\pi\mathrm{i}(h+k)})2\mathrm{i}p_A \sin(2\pi lz). \tag{3}$$

At this point the free parameters are the magnitude of the magnetic moment and the angle to the c-axis. Although we have only three reflections available, there is a point which plays an important role in the calculation. If we compare the calculated and experimental

patterns of the partially resolved reflections (3/2 1/2 1) and (1/2 1/2 3), the agreement is better with the spins lying in the *a–b* plane than with them lying along the *c*-axis.

Therefore, for the canted magnetic structure model the ordered magnetic moments per ion at 2 K are estimated to be $S[\boldsymbol{k}_1] = 1.5(4)\ \mu_B$ ($\boldsymbol{S}(\boldsymbol{k}_1) = 1.5(1)\hat{\boldsymbol{x}} + 0.2(5)\hat{\boldsymbol{z}}$) and $\boldsymbol{S}[\boldsymbol{k}_2] = 1.6(1)\hat{\boldsymbol{y}}\ \mu_B$. The same analysis can be applied at 100, 200 and 300 K, yielding $S[\boldsymbol{k}_1] = \{1.4, 1.2, 1.0\}\ \mu_B$ and $S[\boldsymbol{k}_2] = \{1.6, 1.5, 1.3\}\ \mu_B$ respectively. For the model with the incoherent mixture of domains with the two propagation vectors having the same ordered moment ($S \approx 2\ \mu_B$), the two domains $\boldsymbol{k}_1$ and $\boldsymbol{k}_2$ occupy 41% and 59% respectively of the total volume of the crystal at 2 K.

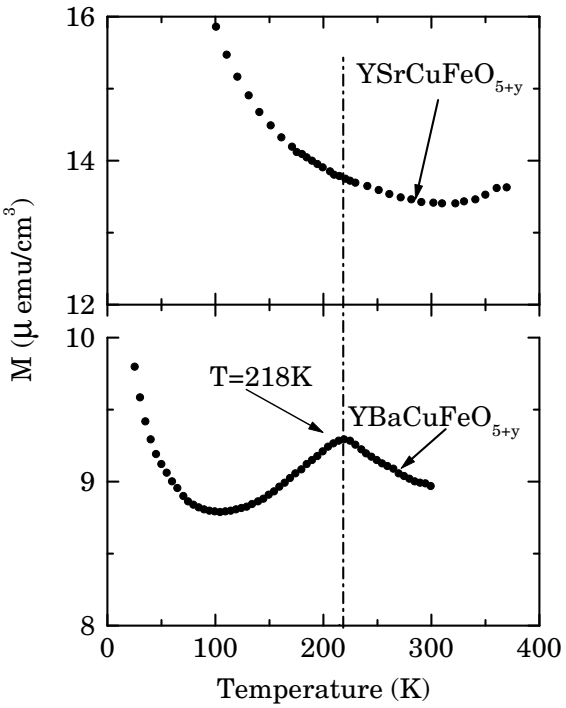

Figure 5. Zero-field-cooled magnetization versus temperature for both $YBaCuFeO_{5+y}$ and $YSrCuFeO_{5+y}$ in a field of 1 kG. There is an increase of the magnetization in the vicinity of the antiferromagnetic transition, but we could not go to higher temperatures due to the limitations of our SQUID.

Figure 5 shows the variation of magnetization with temperature for the $YSrCuFeO_{5+y}$ and $YBaCuFeO_{5+y}$ compounds. For the latter a broad peak is observed at 218 K that can be associated with the satellite peaks in the NPD pattern in that temperature range [2]. No such transition occurs in the case of $YSrCuFeO_{5+y}$, in agreement with the neutron data. We see an increase in the magnetization above 360 K, in the vicinity of the antiferromagnetic phase transition.

5. Mössbauer spectra

Figure 6 shows the Mössbauer spectra (MS) of $YSrCuFeO_{5+y}$ at 450 K (the paramagnetic region) and 4.2 K (the magnetic region). The parameters obtained from least-squares fitting

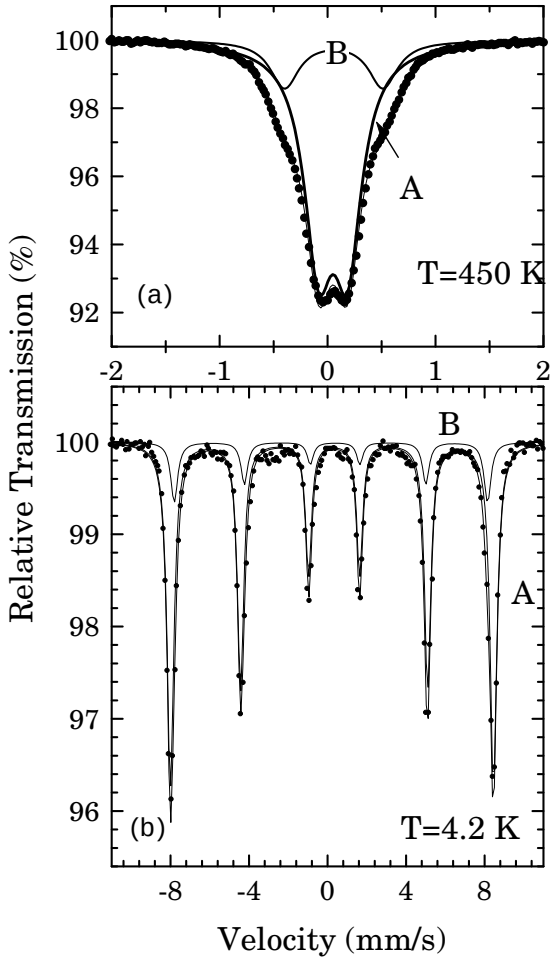

Figure 6. Mössbauer spectra of the $YSrCuFeO_{5+y}$ compound at (a) 450 K and (b) 4.2 K.

Table 2. Experimental values of the half-linewidth $\Gamma/2$ in mm s^{-1}, the isomer shift δ relative to that of metallic Fe at RT in mm s^{-1}, the quadrupole shift ε in mm s^{-1}, the hyperfine magnetic field H in kG and the hyperfine magnetic field spread ΔH modulating the linewidths, as obtained from least-squares fits of the Mössbauer spectra of $YSrCuFeO_{5+y}$. The numbers in parentheses are estimated standard deviations referring to the last significant digit. $\Delta H_A(4.2) = 2$ kG; $\Delta H_B(4.2) = 2$ kG; area of component A $\simeq 85\%$; area of component B $\simeq 15\%$.

T (K)	$\Gamma/2$	δ	ε	H
450	0.174(1)	0.156(1)	0.136(1)	
	0.160(0)	0.164(3)	0.468(1)	
4.2	0.171(2)	0.385(0)	−0.055(1)	513(1)
	0.186(0)	0.381(0)	−0.106(7)	497(8)

using Lorentzian lineshapes are listed in table 2. The 450 K spectrum (figure 6(a)) was analysed with two doublets, denoted by A and B. The presence of two doublets in the MS

is an unexpected result since there is only one crystallographic site for Fe. Component A (85% of the 450 K spectrum) can be attributed to the structurally predicted fivefold-oxygen-coordinated Fe site [5, 8, 15, 16]. A first explanation of the origin of component B is that it comes from an impurity phase. The possibility that component B comes from some iron which replaces the Cu ions in the $Y_2Cu_2O_5$ compound is ruled out because (a) this would mean that all of the Cu in $Y_2Cu_2O_5$ is replaced by Fe, something nearly impossible because $Y_2Fe_2O_y$ does not exist, and (b) for $Y_2Cu_2O_5$, $T_N = 17$ K [22], while the Mössbauer spectra for component B are magnetically split up to 390 K. Having excluded the possibility of an impurity origin for component B, we can attribute it to a second non-equivalent (from the Mössbauer point of view) Fe site in the structure. This can happen either with a part of Fe being octahedrally coordinated (due to some remnant oxygen) or with some Fe at $z \simeq 0.27$ and not at the $z \simeq 0.25$ position (structural model III)—that is, at a site normally occupied by Cu. A third explanation consists in having Cu and Fe in different (successive) layers with a small amount of Fe residing in the copper plane (structural model II).

The 4.2 K MS (figure 6(b)) seems from a first viewing to consist of a component with inhomogeneous broadening. However, the small asymmetry between lines 1 and 6 dictates the introduction of a second site. Taking as a guide the 450 K spectrum, we fitted the 4.2 K spectrum with two sextets, with spectral area ratio 85:15. It is worth noticing that at 4.2 K the hyperfine field of the majority component A is 16 kG greater than that of component B.

Next, we calculated the angle between the iron magnetic moment $\langle \boldsymbol{S} \rangle$ and the principal electric field gradient (EFG) axis from the values of ε at 450 K and 4.2 K (for both components A and B). The principal axis of the EFG tensor is along the c-axis and, supposing that $\eta = 0$ (an assumption supported by the tetragonal symmetry) and that $q = V_{zz}/e$ is positive (as indicated from a point charge calculation of V_{zz}), then the equation

$$\varepsilon(4.2\ \mathrm{K}) = \varepsilon(450\ \mathrm{K})(3\cos^2\theta + 1)/2$$

gives $\theta_A = 75^\circ \pm 2^\circ$ and $\theta_B = 65^\circ \pm 2^\circ$ ($\varepsilon = (1/8)e^2qQ(3\cos^2\theta - 1 + \eta\sin^2\theta\cos 2\phi)$ and $\varepsilon = (1/4)e^2qQ(1 + \eta^2/3)^{1/2}$ for the magnetic and paramagnetic spectra respectively). In $YBaCuFeO_{5+y}$ the magnetic moment makes an angle of 68° with the c-axis (if $q > 0$).

In order to determine the transition temperature, we recorded the relative transmission of the 14.4 keV γ-rays of ^{57}Co at zero velocity as a function of temperature. In the paramagnetic region there is a decrease of the zero-velocity transmission due to the 10% absorption (at $v = 0$) of the unresolved doublet. When the spectrum becomes magnetically split, absorption occurs at non-zero velocities. This method is a thermal scan method in Mössbauer spectroscopy for determining the ordering temperature. So, this measurement allows the determination of the transition temperature from the paramagnetic to the magnetically ordered state. In figure 7 the variation of the relative transmission with temperature is shown. The transition temperature T_N is defined as the intersection of the maximum-slope line of the curve with the extrapolation from the high-temperature region. It can be seen that $T_N = 397 \pm 5$ K and that the transition to the magnetically ordered state is not very sharp, since the relative transmission is saturated 59 K below T_N. However, because of the overlapped nature of the subspectra and the manner in which splitting first occurs, the observed broadness of the transition is rather indicative. Of course the smearing out of the transition in the region close to T_N can be attributed to variations of the average concentration Cu:Fe = 1:1 through the volume of the crystallites. Such inhomogeneities in the crystallites can produce regions with somewhat different Néel temperatures. In the parts of the crystallites with higher T_N, $\langle S_i \rangle$ is non-zero even when a large part of the antiferromagnetic material has already gone into the paramagnetic state. The result is a broad transition that occurs over a certain range of temperatures which form a Néel region.

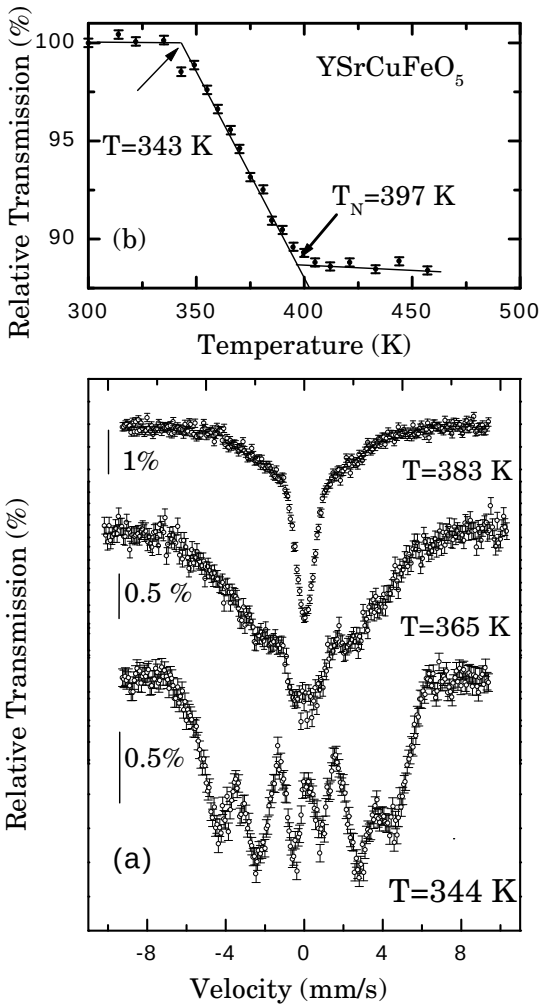

Figure 7. (a) The temperature dependence of the zero-velocity relative transmission. The change in transmission at T_N results from the absence of magnetic splitting above T_N. The transition temperature T_N is defined as the intercept of the extrapolation of the curve at the maximum slope with the temperature axis. (b) Mössbauer spectra in the vicinity of T_N.

For $T < T_N$ the spectra consist of a sextet with broad absorption lines. For $350 \leqslant T \leqslant 413$ K (figure 7(b)), the spectra indicate relaxation behaviour, similarly to the case for the $YBaCuFeO_{5+y}$ compound [8]. For $T < 350$ K the MS show an asymmetric broadening which decreases as the temperature is reduced. A first attempt to fit the spectra with Lorentzian lines supposing that the hyperfine magnetic field follows a Lorentzian distribution gave poor results. The ^{57}Fe MS provide information about the magnitude and the polarization of the s-electron wave functions at the ^{57}Fe nuclei. These charge and spin densities depend on the environment of the Fe atom. Therefore, the asymmetry can be attributed to the cationic surrounding of the Fe, which can create appreciable changes in the hyperfine magnetic field. Due to the different possible configurations, complex magnetic MS can be expected. The MS should consist of several components whose H_{eff} varies linearly

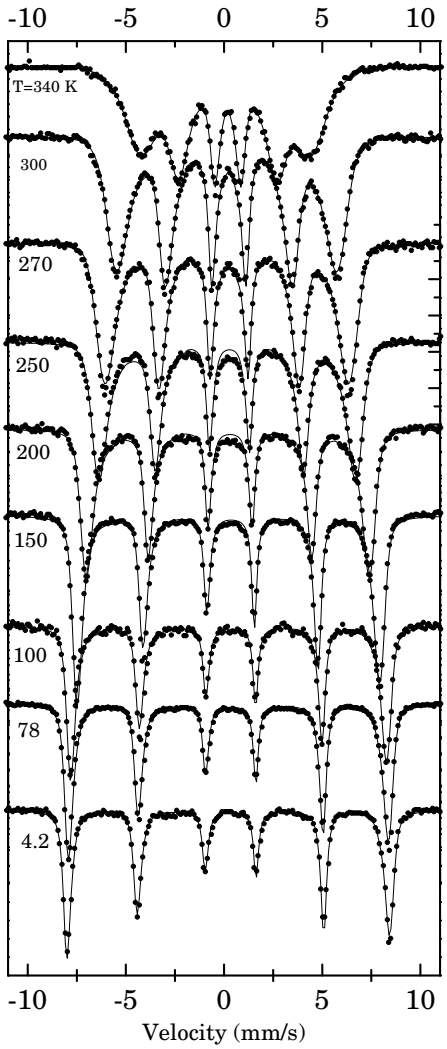

Figure 8. Mössbauer spectra of $YSrCuFeO_{5+y}$ from 340 K down to 4.2 K. The continuous line is the fit to the experimental spectra assuming a distribution of the effective hyperfine magnetic fields.

with the number of nearest iron neighbours. The weight of each subcomponent will be given by a binomial distribution, if short-range-order phenomena are absent. The structure of the spectra due to disordering is not well resolved, due to the poor inherent resolution of the Mössbauer spectroscopy (≈16 kG). Drastic changes of the hyperfine parameters are observed only when different Fe coordinations are present. Applying the above discussion, we have replaced the multicomponent analysis with an H_{eff} that follows a distribution $p(H_{eff})$ which modulates the absorption lines. For the estimation of the distribution we used the Le Caër–Dubois program [23]. Figure 8 shows the fitted MS from 340 K down to 4.2 K. Figure 9 shows the corresponding distributions of the magnetic hyperfine field for several temperatures as estimated from the Le Caër–Dubois program. The small tail to the left of the maximum of $p(H_{eff})$ corresponds to component B. The hyperfine magnetic

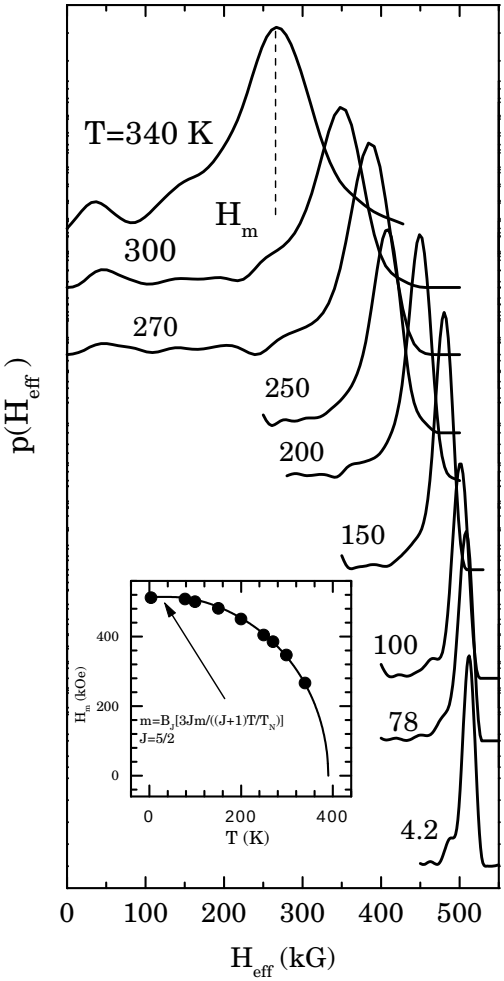

Figure 9. The estimated hyperfine-field distribution lineshape $p(H_{eff})$ for the Mössbauer spectra of YSrCuFeO$_{5+y}$ as a function of temperature. The inset shows H_m, defined as the point at which $p(H_{eff})$ has a global maximum, as a function of temperature.

field, defined as the maximum in $p(H_{eff})$, is plotted as a function of the temperature in the inset of figure 9. This particular value represents the larger percentage of Fe ions in the sample. The parameters obtained are very close to those obtained upon fitting the spectra with two sites and considering that the hyperfine field follows a Lorentzian distribution. For the estimation of $p(H_{eff})$ we considered all of the components of the spectrum as having isomer shifts $\delta \approx 0.28$ mm s^{-1} and $\varepsilon \approx -0.06$ mm s^{-1}. The continuous line in the inset of figure 9 is obtained from the mean-field approximation by solving the equation

$$\sigma = B_J[(3J)/(J+1)(\sigma/\tau)]$$

where $\sigma = H_{eff}(T)$ is the effective hyperfine field, $\tau = T/T_N$ is the reduced temperature and J is the spin of Fe in the high-spin state ($J = 5/2$).

6. Discussion

6.1. Mössbauer spectra

Near T_N, we have the coexistence of magnetically split and paramagnetic spectra. In this temperature range, the Weiss molecular field may offer a reasonable explanation of the Mössbauer spectra. In this context, the electron spin jumps in a random manner between the discrete spin states, as a result of the interactions with local fluctuating fields. Due to disordering phenomena among the Cu and Fe, we have strong local (short-wavelength) fluctuations of the hyperfine magnetic field near T_N. At low temperatures the spin-wave frequency is large compared to the Larmor precession frequency and therefore H_{eff} is proportional to $\langle S_z \rangle$. Thus, the observed broadening should be of static origin.

6.2. Magnetic structure

The presence of two propagation vectors $\boldsymbol{k}_1$ and $\boldsymbol{k}_2$ for $T < T_N$ has been observed in oxygen-reduced $PrBaCuFeO_{5+y}$ [5]. In $YBaCuFeO_{5+y}$ for $T \leqslant T_{N1} = 441$ K the magnetic structure is described with propagation vector $\boldsymbol{k}_1$ (references [24, 6, 10]), while for $T \approx 200$ K a commensurate-to-incommensurate magnetic transition occurs. The propagation vector for the incommensurate cell is (0, 0, 0.213). We must note at this point that the incommensurate magnetic structure could not be interpreted with a magnetic-domain-based model (for the validity of this argument see below). In contrast to that of $YBaCuFeO_{5+y}$, the magnetic structure of the $YBaCuCoO_{5+y}$ compound for $T < T_N$ can be described only with $\boldsymbol{k}_1$, $p_A = p_B$ (because $z = 0.2763$, the other case, $p_A = -p_B$, can be ruled out) and with the ordered magnetic moment parallel to the c-axis [25]. For the solid solution $YBaCu_{2-x}Co_xO_{5+y}$ ($0.3 \leqslant x \leqslant 0.75$) the magnetic structure is described with $\boldsymbol{k}_2$ and with the ordered magnetic moment lying in the a–b plane, whereas for $0.75 \leqslant x \leqslant 1$ the magnetic structure is described with $\boldsymbol{k}_1$ (the magnetic moment along the c-axis for $T_2 \leqslant T \leqslant T_3$ and away from the c-axis for $T < T_2$) [26]. Finally, for $YBaCoCu_{0.5}Fe_{0.5}O_5$ the superlattice magnetic peaks come from a magnetic structure with propagation vector $\boldsymbol{k}_2$ [27].

In the Pr compound the presence of two propagation vectors originates from some kind of interaction between (Cu, Fe) and Pr ions; thus, in the case of $YSrCuFeO_{5+y}$ such an explanation is not applicable, since Y^{3+} does not carry a magnetic moment. The same holds for $YBaCuFeO_{5+y}$. The existence of site B in the MS of $YSrCuFeO_{5+y}$, $PrBaCuFeO_{5+y}$ and $YBaCuFeO_{5+y}$ compounds (although it was either ignored or attributed to a secondary phase in the case of $YBaCuFeO_{5+y}$) leads us to believe that there might be a correlation between site B and the two propagation vectors. As previously noted in the description of the MS, site B arises from octahedrally coordinated iron ions due to remanent oxygen at the O4 sites which mediate in creating exchange interactions between nearest-neighbour (Cu, Fe) ions. If the O4 site was completely empty only dipolar interactions would exist. Consequently, the existence of the additional oxygen creates, in addition to the dipolar ones, superexchange interactions of the (Cu, Fe) ions that are located above and below the Y layers. Such a complicated spin Hamiltonian, can probably explain the two-propagation-vector magnetic structure. In the case of $YBaCuFeO_{5+y}$ the amount of additional oxygen is so small that it is not able to stabilize the $\boldsymbol{k}_2$-component in a long-range order.

7. Conclusions

This study shows that $YSrCuFeO_{5+y}$ magnetic structure can be described with two propagation vectors $\boldsymbol{k}_1 = [\frac{1}{2}, \frac{1}{2}, \frac{1}{2}]$ and $\boldsymbol{k}_2 = [\frac{1}{2}, \frac{1}{2}, 1]$. The local structure of Fe, as seen through the Mössbauer spectra, is not unique. The majority of the iron occupies a site with pyramidal oxygen coordination, while 15% occupies a site with octahedral oxygen coordination. The second site may be related to the appearance of $\boldsymbol{k}_2$. The amount of additional oxygen in the $(\frac{1}{2}, \frac{1}{2}, \frac{1}{2})$ oxygen position should play a critical role in this. The x-ray and neutron powder diffraction data show a simple average structure, although in reality the microstructure of $YSrCuFeO_{5+y}$ can be more complicated (comprising 90° domains which are responsible for site B).

Acknowledgments

Partial support for this work was provided by the EC through the CHRX-CT93-0116, Human Capital and Mobility Programme (access to large-scale facilities) projects.

References

[1] Er-Rakho L, Miceli C, Lacorre P and Raveau B 1988 *J. Solid State Chem.* **73** 531
[2] Prassides K, Christides C, Lappas A and Mombru A 1992 *ISIS Experimental Report* RB/3545
[3] Mombru A W, Prassides K, Christides C, Erwin R, Pissas M, Mitros C and Niarchos D 1998 *J. Phys.: Condens. Matter* **10** 1247
[4] Kallias G, Pissas M, Christides C, Sonntag R and Niarchos D 1997 *Physica* B **234–236** 608
[5] Pissas M, Kallias G, Psycharis V, Gamari-Seale H, Niarchos D, Simopoulos A and Sonntag R 1997 *Phys. Rev.* B **55** 397
[6] Caignaert V, Mirebeau I, Bouree F, Nguyen N, Greneche J-M and Raveau B 1995 *J. Solid State Chem.* **114** 24
[7] Voughey J T and Poeppelmeier K P 1991 *Proc. Int. Conf. on Chemistry of Electronic Ceramic Materials (Jackson, WY, 1990) (NIST Special Publication 804)* ed P K Davies and R S Roth (Washington, DC: US Department of Commerce) p 419
[8] Meyer C, Hartman-Boutron F, Gros Y and Strobel P 1990 *Solid State Commun.* **76** 163
[9] Pissas M, Mitros C, Kallias G, Psycharis V, Simopoulos A, Kostikas A and Niarchos D 1992 *Physica* C **192** 35
[10] Mombru A W, Christides C, Lappas A, Prassides K, Pissas M, Mitros C and Niarchos D 1994 *Inorg. Chem.* **33** 1255
[11] Atanassova Y K, Popov V N, Bayachev G G, Iliev M N, Mitros C, Psycharis V and Pissas M 1993 *Phys. Rev.* B **47** 15 201
[12] Wiles D B and Young R A 1981 *J. Appl. Crystallogr.* **14** 149
[13] Rodríguez-Carvajal J 1990 FULLPROF: a program for Rietveld refinement and pattern matching analysis *Satellite Mtg on Powder Diffraction to the 15th Congr. of the IUCr (Toulouse, 1990)* abstracts, p 127
[14] Shannon R D 1976 *Acta Crystallogr.* A **32** 751
[15] Pissas M, Kallias G, Poulakis N, Niarchos D, Simopoulos A and Liarokapis E 1995 *Phys. Rev.* B **52** 10 610
[16] Pissas M, Kallias G, Moraitakis E, Niarchos D and Simopoulos A 1994 *Physica* A **234** 127
[17] Kim J S, Lee J Y, Swinnea J S, Steinfink H, Reiff W M, Lightfoot P, Pel S and Jorgensen J D 1991 *J. Solid State Chem.* **90** 331
[18] Pissas M, Mitros C, Niarchos D, Kostikas A, Simopoulos A, Abrashev M, Hadjimitov V and Iliev M 1994 *Phys. Rev.* B **50** 10 157
[19] Lyons D H, Kaplan T A, Dwight K and Menyuk N 1962 *Phys. Rev.* **126** 540
Miceli P F, Tarascon J M, Greene L H, Barboux P, Giroud M, Neumann D A, Rhyne J J, Schneemeyer L F and Waszczak J V 1988 *Phys. Rev.* B **38** 9209
Kadowaki H, Nishi M, Yamada Y, Takeya H, Takei H, Shapiro S M and Shirane G 1988 *Phys. Rev.* B **37** 7932
Mirebeau I, Suard E, Caignaert V and Bouree F 1994 *Phys. Rev.* B **50** 3230

Shamoto S, Sato M, Tranquada J M, Sternlieb B J and Shirane G 1993 *Phys. Rev.* B **48** 13 817
[20] Rossat-Mignod J 1987 *Methods of Experimental Physics* (New York: Academic) p 69
[21] Watson R E and Freeman A J 1961 *Acta Crystallogr.* **14** 27
[22] García-Muñoz J L, Obradors X and Rodríguez-Carvajal J 1995 *Phys. Rev.* B **51** 6594
[23] Le Caër G and Dubois J M 1979 *J. Phys. E: Sci. Instrum.* **12** 1083
[24] Pissas M, Mitros C, Kallias G, Psycharis V, Niarchos D, Simopoulos A, Kostikas A, Christides C and Prassides K 1991 *Physica* C **185–189** 553
[25] Huang Q, Karen P, Karen V L, Kjekshus A, Lynn J W, Mighell A D, Sora I N, Rosov N and Santoro A 1994 *J. Solid State Chem.* **108** 80
[26] Barbey L, Nguyen N, Caignaert V, Studer F and Raveau B 1994 *J. Solid State Chem.* **112** 148
[27] Barbey L, Nguyen N, Ducouret A, Caignaert V, Greneche J M and Raveau B 1995 *J. Solid State Chem.* **115** 514